Applied Composite Materials (2023) 30:1979–1999
https://doi.org/10.1007/s10443-023-10157-1

Investigating Damage Mechanisms in Cord-Rubber Composite Air Spring Bellows of Rail Vehicles and Representative Specimen Design

J. Torggler[1] · A. Dutzler[2] · B. Oberdorfer[3] · T. Faethe[2] · H. Müller[4] · C. Buzzi[1] · M. Leitner[1]

Received: 14 December 2022 / Accepted: 2 August 2023 / Published online: 22 August 2023

Abstract
Cord-rubber materials are used in crucial components of rail vehicles, such as air spring bellows in secondary suspension. A detailed understanding of the material behaviour of these components is thus of the utmost importance at an early stage of development. In general, a minor knowledge of the fatigue behaviour is currently all that is available today, while empirical methods involving designer experiences are in most cases essential requirements for this work. The design can be carried out more efficiently based on a representative cord-rubber composite specimen than on an entire air spring bellow. In this paper, the design of such representative specimens is shown taking different geometries and test conditions into consideration. It is found, that a flat specimen design is suitable for analysing the base material under different loading scenarios. The design and optimisation of the specimen geometry was carried out using finite element analysis, which was validated by means of optical strain measurement. The test procedure for the specimen was designed to provide a sound transferability to experimental testing of the components. A fracture pattern study was carried out using radiography and micro computed tomography. The results show, that the dominant damage mechanism is the separation of the layers from each other, denoted as delamination. In conclusion, the developed specimen is well suited for further investigations of the composite material. Furthermore, it will significantly accelerate the development of new air springs and new layups in particular. Future work will focus on a systematic investigation of the fatigue behaviour of the cord-rubber composite air-spring bellows based on the fatigue data of the representative specimens designed in this work.

Keywords Cord-rubber composite · Damage mechanisms · Fatigue testing · Delamination · Finite element analysis · Tomography

✉ J. Torggler
julian.torggler@tugraz.at

[1] Institute of Structural Durability and Railway Technology, Graz University of Technology, Inffeldgasse 25/D, 8010 Graz, Austria

[2] Siemens Mobility Austria GmbH, Eggenberger Straße 31, 8020 Graz, Austria

[3] Strahlenmesstechnik Graz, Steyrergasse 17, 8010 Graz, Austria

[4] GMT Gummi-Metall-Technik GmbH, Liechtersmatten 5, 77815 Bühl, Germany

1 Introduction

Reinforced rubber materials are used in many industrial applications, including mobility applications [1, 2]. A very well-known and relevant application of reinforced rubber materials is the tire [3–5]. Very similar materials and material designs are used in the spring stage for high comfort applications or for level control. These air suspension systems are used in both cars and trucks to provide the vertical suspension [6–8].

It is also common to use air spring systems, in the bogie of a rail vehicle for passenger coaches and traction units as secondary spring stages (needed for high comfort requirements or high payloads [9]). In this case, it connects the vehicle body and the bogie and facilitates the spring effect through the compressibility of the air. In addition to pure vertical suspension, lateral and, if necessary, longitudinal and torsional suspension must also be provided. For this reason, the load situation differs from that in car and truck applications. In addition, the components are manufactured in a near-series production in much smaller quantities and have a larger dimension. This may lead to manufacturing effects on the resulting in-service life.

Using finite-element analysis, it is possible to estimate static quantities for these fibre-reinforced composites [10]. These support the design in terms of load capacity. Several fatigue life studies with many component tests have been carried out for trucks, buses and automotive applications [8, 11–13]. However, in these similar applications, the components are loaded in a completely different way to that of the railway application. A reliable service life prediction for railway application air spring bellows is not known, available or accessible. This can result in time consuming and costly development and with the need for multiple prototypes.

The focus of this work is on the composite material of a railway air spring bellows. The composite material consists of reinforcing fibres of polyamide embedded in a matrix of a rubber mixture. The damage behaviour of cord-rubber composites is of a comparatively special character. Depending on the load, different damage mechanisms can occur, which basically do not occur in this form in any of the base materials [7, 11]. One of these specific damage mechanisms is delamination. It is characterised by the loss of adhesion between the matrix (elastomer) and the fibres or an entire layer [14].

Due to the higher component costs of air spring systems in rail vehicles as also the significantly higher efforts required for experimental testing of entire components, this paper presents a methodology for designing small-scale representative specimens that exhibit similar damage mechanisms to those of the components. Based on these representative specimens, an efficient experimental study of the fatigue behaviour under a variety of load conditions is enabled, where the transferability of the results from small- to large-scale is of the utmost importance. Therefore, the main task is to design the specimen to ensure transferable design values.

Standardised specimens, such as the tension test specimen for rubber [15], are only one possibility for this task. It must be clearly defined what is to be investigated by means of the test specimen. There are different approaches for fibre composite specimens. The single fibre is tested to determine the mechanical properties of the fibre [16–19]. Pull-out tests of the fibre can be performed to determine the adhesion between fibre and matrix [20, 21]. A cord rubber specimen with three fibres has been developed in [22]. A strip for uniaxial testing of the composite was used in [5, 23–25]. To study the biaxial behaviour of the material, an Arcan-like specimen can be used [26–29].

Table 1 Specifications for the rubber mixture, [10]

Characteristic	Value	Unit	Test Standard
Density	1,13-1,16	g/cm^3	DIN 1183 T1
Flexibility of Shock	36-42	%	DIN 53 512
Tear-Growth Resistance	Min. 12,5	MPa	DIN 53 504
Elongation at Break	Min. 370	%	DIN 53 504

Table 2 Properties of polyamide, [10]

Type	Tensile strength in MPa	Young's modulus in GPa	Density in g/cm^3
Polyamide fibre	~ 950	~ 6	1,14
Compact polyamide	75–94	1,6–3,7	1,14

The focus of this work is to derive a representative flat specimen from the air spring bellow used in railway vehicles. This paper shows how the mechanism(s) leading to delamination can be better illustrated.

2 Materials

A composite of cord fibres (polyamide PA) and rubber mixture is used as the material under investigation in this study. A natural rubber mixture is used as the matrix material for the cord fibre, which is applied by calendering. Prior to this process, the fibre is dipped in a bonding agent, which, however, is not included in the modelling due to its low thickness. The high strength fibres take over the mechanical loads and the matrix supports and positions the fibres in the given position. There is an additional layer of synthetic rubber mixture on the inside and outside of the bellows wall to ensure tightness on the inside and better corrosion resistance on the outside. Table 1 shows the key data of the rubber mixture used as the matrix material for the fibres.

Table 2 presents the mechanical properties of compact polyamide compared to the polyamide fibre. The tensile strength of the fibre is significantly higher than the base material with simultaneous higher young´s modulus.

3 Damage Mechanisms in Air Spring Bellows

Figure 1 shows a CAD view of a typical long-distance passenger coach bogie. The component highlighted is the secondary spring stage, which connects the car body to the bogie. Such a secondary spring stage consists of an air spring bellow and an emergency spring device.

The spring effect due to the compressibility of the air is used in the air spring bellow. Movements in the chassis during different driving conditions also need to be balanced. Figure 2 (left) shows the movement in the secondary spring stage during cornering. Therefore, in addition to pure vertical suspension, lateral, and if necessary, longitudinal and torsional suspension must also be provided. As shown in Fig. 2 (right), there are several loads acting on the air spring bellow in addition to the internal pressure.

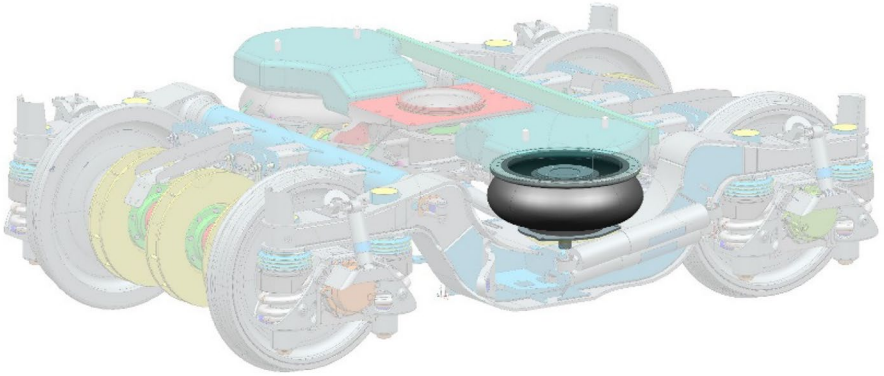

Fig. 1 Secondary spring stage in the rail vehicle bogie [30]

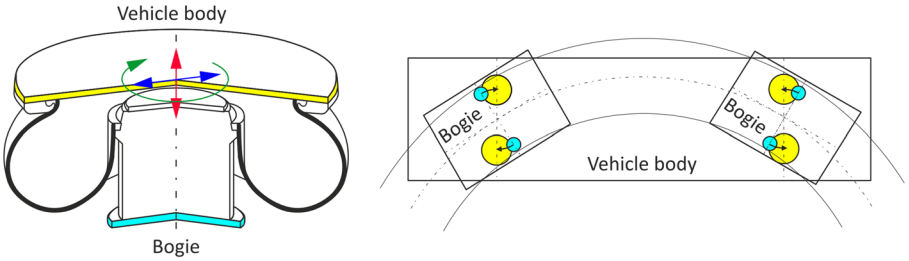

Fig. 2 Loads acting on the air spring bellow (left) and secondary spring stage deflection during cornering (right)

The investigated composite material of the air spring bellows has to withstand many load cycles; the service life of rubber parts amounts at least 6 years (the service life can be also up to 12 years). Unexpected damage or failure is expensive and problematic. The tests required by the standard on the secondary spring system are usually carried out by the manufacturer up to a certain number of load cycles [31]. These validation tests ensure, that the component generally meets this requirement. However, tests to failure are the focus of such experiments and are therefore rarely performed.

Various types of damage can occur in air spring bellows, such as bursting, cracking of the elastomer matrix or delamination. Component test data is available from previous work [32], where various internal pressure loads and lateral deflections were tested. Component tests of an air spring system used in railway applications with a relevant scope are basically neither available nor accessible in the literature. Using the developed FE-Model [10] the aim was the to convert of the pressure-life (p-N) curves from the service life tests into a stress-life (S–N) curve. This was not possible due to the small data base.

The evaluation of this series of tests and operating experience shows a clear result, as the primary damage is delamination (in both cases over 60% of the damage). Figure 3 (left) shows the structure inside an air spring bellow. The elastomer matrix material is concealed, revealing steel cores and polyamide fibres. To the right of Fig. 3 is a section through a typical case of delamination in the air spring bellow.

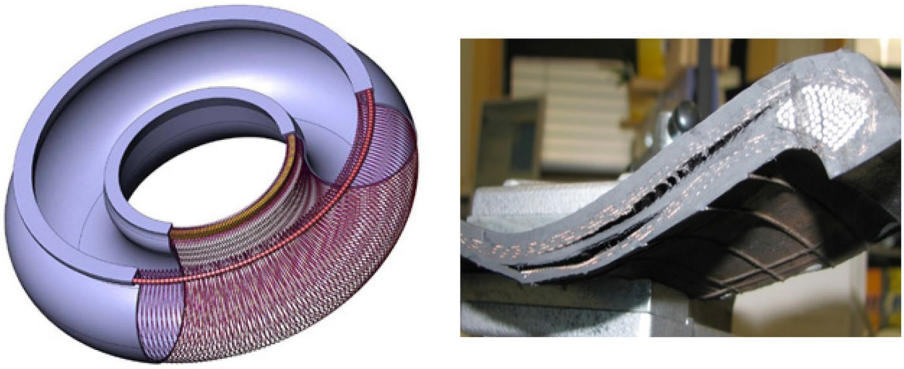

Fig. 3 Air spring bellow interior (left) and air spring bellow delamination (right)

In order to characterize the most common failure mechanisms, the local positions where the damage occurred during the test were examined by the developed FE-Model [32]. Some characteristic features of the different mechanisms were observed.

Symmetrical tensile loads on the strength member were observed at the locations where a crack was detected in the elastomer. There was also a large change in layer angle to each other and a small change in fibre elongation.

The most common mechanism, delamination, shows an asymmetric tensile or compressive load on the strength member. The change in ply angle to each other was small and a high change in fibre elongation was observed.

Based on the fibre structure visible in Fig. 3, these findings are illustrated in the schematic sketch in Fig. 4. The undeformed state is shown in grey and the deformed states are shown in red and blue.

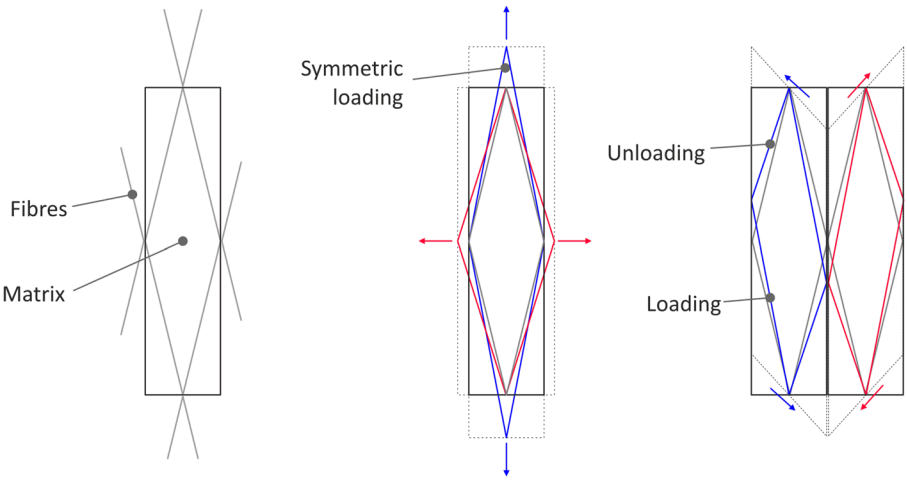

Fig. 4 Characteristics for mechanisms, undeformed (left), crack in the elastomer (middle) and delamination (right)

To better understand the damage mechanisms within the material, the idea is to develop a material specimen. The task is to adapt a specimen geometry to investigate the dominant damage mechanism in testing and in the field, delamination.

According to several sources [7, 33], the causes are the loss of adhesion between the fibre and the elastomer as well as fatigue of the elastomer. If the minimum load on the fibres is close to full unloading (or compression) under lateral or torsional loading of the bellow, the service life is significantly reduced [6, 34]. This can lead to a loosening of the fibre interlacing, resulting in a different fibre surface geometry. The increased load on the fibre and rubber connection can lead to delamination.

4 Specimen Development

Several concepts were considered. One idea was to use small series or industrial components. Initial simulations of typical components such as sleeve bellows (used for vibration isolation) showed, that it is not possible to transfer the loading of the bellow to these components. The clamping of these bellows was also problematic, as the connecting parts were designed for significantly lower loads.

Figure 5 shows the shortlist of the concepts considered for specimen geometries.

Standardised test specimens are considered, like in DIN EN ISO 527 [35] specified dimensions for the multipurpose test specimens. Depending on the fibre orientation, a strong tensile load acts on the fibres and there is small change in the angle of the layers to each other. Therefore, it is not possible to make a statement about the type of fatigue crack in the elastomer. Typical fibre orientations in the air spring bellow are between 10° and 30° with respect to the specimen longitudinal direction of the specimen. As shown in the figure for the multipurpose test specimen on the right, only very small fibre angles show continuous fibres throughout the specimen. Therefore, this specimen geometry is not suitable for the intended experiments.

One of the first concepts is a tubular specimen, which is similar to the geometry bellow. When a tensile load is applied to the tube, it acts purely on filaments. There is a small change in the angle of the plies to each other, therefore no statement is possible about the crack in elastomer. When torsion is applied to the tube, simultaneous loading and unloading of fibre layers occurs, which allows a statement to be made about delamination. Several issues must be additionally clarified here, however, such as the clamping of the specimen, the manufacturing effort, the discontinuity points with overlapping layers, the influence of thickness/distance between layers, the influence of curvature and geometry dependent results.

Concepts for specimen	Sleeve bellows	Multipurpose specimens	Tube sample	Flat sample	Arcan-like sample
Sketch/illustraion		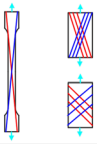	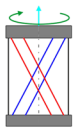	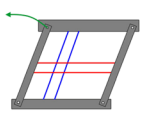	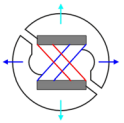
# of test setup axes	2	1	2	1	2
Type of damage	Crack in elastomer/delamination	-	Delamination	Crack in elastomer	Delamination

Fig. 5 Different approaches to specimen development

Another concept was a flat specimen. Two different designs were investigated, with the aim of investigating the type of damage in the elastomer matrix or delamination. The first design, a rectangular specimen, has a fixed clamp on all four sides, connected by pivoted points. This design is intended to provide a large change in the angle of the layers to each other and a small change in fibre elongation. The challenge is in to clamp this specimen, as both fibre directions require a pre-tensioning.

The other flat specimen concept was designed to investigate delamination as the dominant damage mechanism. A small change in ply angle to each other and a large change in fibre elongation were to be realised. The specimen developed follows an Arcan-like specimen [27, 29].

Main issues, such as clamping, manufacturing effort and mapping of relevant damage mechanisms have led to the implementation of the Arcan-like flat specimen, which best meets these requirements. The literature search revealed that no shear test data were available or accessible for the material under consideration, making this specimen geometry interesting for biaxial testing. Figure 6 on the left shows the Arcan like flat specimen geometry, the clamping area is indicated in the image as a grey bar. The coordinate system used for the flat specimen is also marked, together with the fibre orientation. The developed flat specimen geometry allows it to cover a fibre angle from ± 0 to ± 35 degrees and 2 to 8 layers of rubberized cord mat. The first specimens were produced with 2 layers of rubberized cord mat at ± 15 degrees.

The test specimen was manufactured as close as possible to the air spring bellow. Figure 6 on the right shows the layup for the manufactured specimen with two layers of rubberized fibre mat in $\pm 15°$. In agreement with the manufacturer, the specimen is realized as a flat specimen with vulcanised steel clamping plates. The clamping plates and the various layers of the specimen are placed in a negative mould and then vulcanized together (see Fig. 7, left) at 160 °C for 20–30 min. The process parameters for the production of the flat specimen were chosen to achieve as similar a state of vulcanisation as possible.

The special properties of the polyamide fibres are shown in the force–elongation diagram in Fig. 7, right. When tension is applied, the initial load curve of a single fibre is the upper envelope in this diagram. With repeated loading of the fibre, a near steady state is reached. To obtain such a diagram, it is first necessary to perform several oscillation tests in the direction of tension under force control [36]. A clear hysteresis and a strong permanent deformation can be observed in the diagram. Air spring bellows are not loaded once

Fig. 6 Arcan-like specimen geometry (left) and specimen confection/layup (right)

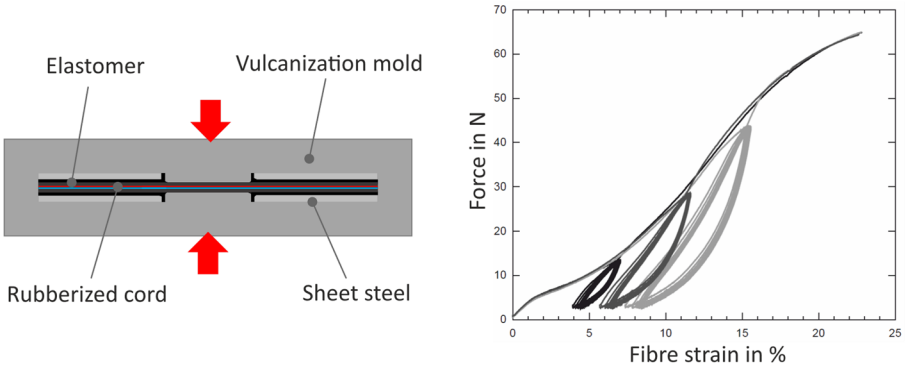

Fig. 7 Vulcanisation (left) and cyclic tensile test on polyamide fibre (right) [36]

only, but repeatedly, so the initial load curve is of minor relevance to the component properties under consideration. What is interesting is the behaviour after several load cycles, e.g. a minimum number of 20. The slope of the steady state hysteresis curves in tension is relevant to the material model for a single fibre.

5 Numerical Simulation of the Fibre-Reinforced Flat Test Specimen

The finite element (FE) simulation of the air spring bellow was the subject of previous work [10], focusing on the component stiffnesses. The developed and validated FE-Model of the air spring bellow was subsequently used to investigate the damage mechanisms [32]. Based on the findings of this work, the present flat specimen was developed. Using a validated simulation model of the air spring bellow, the stress on the fibre can be evaluated in the areas, where the damage was detected. The stresses determined in the air spring bellow can thus be transferred to the specimen geometry.

The aim of the numerical simulation is to develop and optimise a small specimen geometry for the fibre composite material. The results shown below refer to the implemented specimen geometry resulting from this development with several iterations.

A numerical simulation of the flat test specimen is carried out using the finite element method. The two-dimensional plane stress model consists of 5621 nodes and 5472 quad elements with linear shape functions, see Fig. 8 (left). Due to the plane stress formulation, the volumetric constraint from the material incompressibility is directly incorporated into the out of plane component of the deformation gradient in an analytic way [37]. Both the lower and upper end edges of the free surface of the test specimen are treated as rigid boundaries. The lower boundary is fixed in space, while on the upper boundary is subjected to the external tensile and shear displacements.

The material behaviour can be simulated using different types of models. For the fibre-reinforced rubber composite, the framework of a transversely isotropic material with two fibre families [38, 39] is used with an anisotropic hyperelastic material formulation. The hyperelastic model is capable of representing a nonlinear elastic, isotropic and incompressible material behaviour. The strain energy is composed of two parts, the first resulting from the matrix and the second from the reinforcing fibres (see Eq. (4)).

The constitutive material behaviour of the rubber matrix is defined by a first strain invariant, isotropic incompressible hyperelastic material formulation. It is based on the

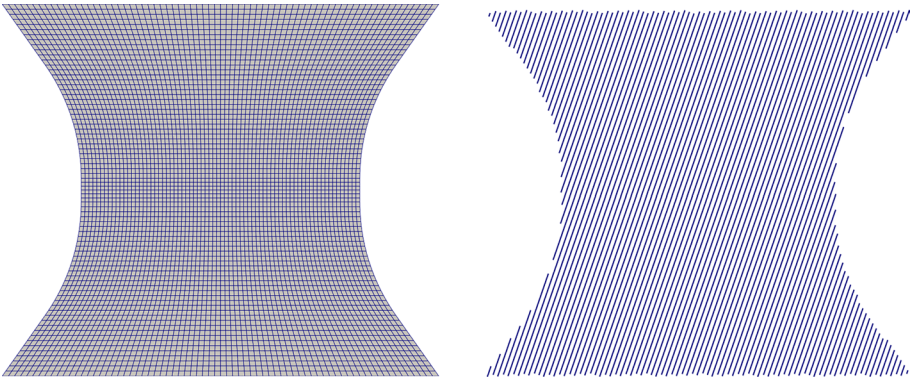

Fig. 8 Two-dimensional quad mesh for the simulation model (left) and a line mesh to visualise the results for one fibre layer (right)

Seth–Hill [40, 41] strain-stretch relation as given in Eq. (1), where E is the strain in the direction of the stretch λ. For the rubber matrix, the strain exponent k is chosen as two, which recovers the Neo-Hookean material formulation from Eq. (2), based on the three principal Green–Lagrange [37] strain values E_1, E_2 and E_3.

$$E(\lambda, k) = 1/k\left(\lambda^k - 1\right) \tag{1}$$

$$\psi_{rubber} = 2\mu/k\left(E_1 + E_2 + E_3\right) \tag{2}$$

The polyamide fibre is defined by an anisotropic hyperelastic material formulation in terms of the fibre normal stretch λ_f. The anisotropic strain energy density function $\psi_{fibre\text{-}layer}$ is formulated as a quadratic dependence of the fibre's normal strain, see Eq. (3). In contrast to the rubber matrix, the strain exponent k_f of the fibre's strain measure is set to one in order to enable a linear fibre-force per undeformed area versus fibre-stretch relationship. The effective elastic modulus per fibre layer is the product of the number of fibres per unit length n_f divided by the cosine of the fibre angle φ_f, the elastic modulus per fibre E_f and the cross-sectional area of the fibre A_f divided by the out-of-plane thickness of the test specimen t.

$$\psi_{cord-layer} = \left(\frac{n_f}{cos\varphi_f}\frac{E_f A_f}{t}\right)E_f^2(\lambda_f, k_f = 1)/2 \tag{3}$$

The strain energy density per undeformed volume ψ for fibre reinforced hyperelasticity is given by the sum of the contributions from the rubber matrix and all fibre layers, see Eq. (4).

$$\psi = \psi_{rubber} + \sum\nolimits_j \psi_{cord-layerj} \tag{4}$$

where j = 1, n is the number of reinforcing fibre families, which is two in the case of the specimen examined.

The relevant geometric and elastic material parameters for the numerical simulation are summarized in Table 3. The numerical analysis of the specimen performed by an initial tensile loading followed by a shear displacement-controlled deformation. The open source

Table 3 Geometrical and elastic material properties for the simulation of the flat test specimen

Description	Symbol	Value and Unit
shear modulus (rubber)	μ	1 MPa
thickness of the flat test specimen	t	5 mm
angles per layer (fibre)	φ_f	(-19°, + 19°)
elastic modulus (fibre)	E_f	5500 MPa
cross-sectional area (fibre)	A_f	0.08 mm^2
number of fibres per unit length	n_f	0.95 fibres/mm

finite element package FElupe is used for the numerical simulation [42]. The constitutive material behaviour is derived from the strain energy function by automatic differentiation [43, 44]. The deformed test specimen is shown in Fig. 9. Here, the fibre forces from the hyperelastic simulation are mapped onto fibre meshes. Each fibre mesh associated with a layer consists of representative fibres as line elements along the fibre direction, see Fig. 9 (right). Tensile force–displacement characteristics without and with a combined shear displacement and corresponding shear forces are given in.

Table 4 and are shown in Fig. 10.

Figure 9 shows the rubber (left) and fibre (right) stress distributions on the deformed test specimen under a combined tensile and shear displacement ($Fy = 2970$ N,

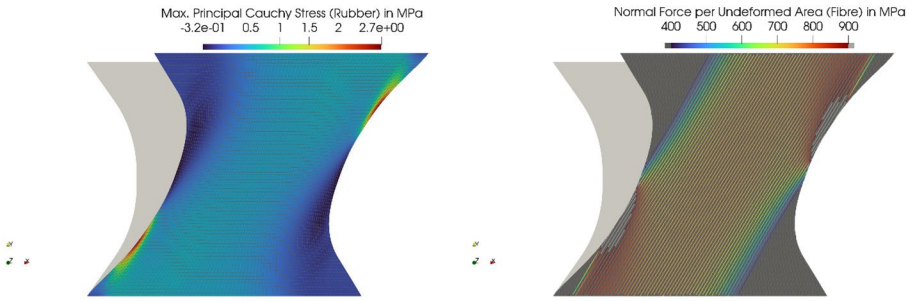

Fig. 9 Finite element modelling of the flat test specimen. Rubber (left) and fibre (right) stress distributions on the deformed test specimen under a combined tensile and shear displacement (Fy = 2970 N, U = 23 mm)

Table 4 Tensile displacement as well as tensile and shear forces of the test specimen

V in mm	F_Y ($U = 0$mm) in kN	F_Y ($U = 23$mm) in kN	F_X ($U = 23$mm) in kN
0.00	0.00	2.21	1.43
1.00	0.48	2.43	1.53
2.00	0.97	2.67	1.64
3.00	1.46	2.93	1.75
4.00	1.97	3.22	1.86
5.00	2.48	3.62	1.97
6.00	2.99	4.10	2.06
7.00	3.51	4.60	2.16
8.00	4.03	5.10	2.25

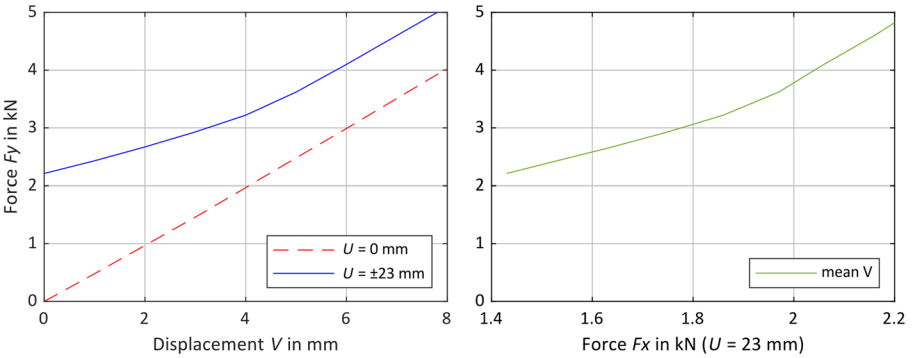

Fig. 10 Characteristic curves as numerical results of the test specimen. Tension force–displacement curves without (red dashed line, left) and with a combined shear displacement (blue solid line, left) and the corresponding shear force (right)

$U = 23$ mm). The uniformity of the stresses in the central region should favour the mechanisms described for the type of damage delamination. An asymmetric tensile or compressive load on the fibre has been realized in this region. At the edge of the specimen, due to geometric effects, there is an exaggeration on one side and a relief on the opposite side. In order to be able to assess the impact of these effects, extensive preliminary tests were carried out with the developed specimen geometry.

The presented FE analysis results have been validated with experimental results. As a first step, the global measurements of force and displacement in the x and y coordinate directions can be used for a first comparison between measurement and simulation. To validate the FE-Model, a camera based optical deformation measurement (the so-called image correlation) was used. The stochastic pattern applied to the specimen surface (see Fig. 11, right) is recorded by a camera during deformation. The displaced pattern in the recorded camera image is identified and the displacements in the component surface are calculated using the measured pixel coordinates. The images were captured using a Basler acA2000-50gm industrial camera and a TechSpec telecentric lens. In Fig. 11 on the left shows the measurement setup.

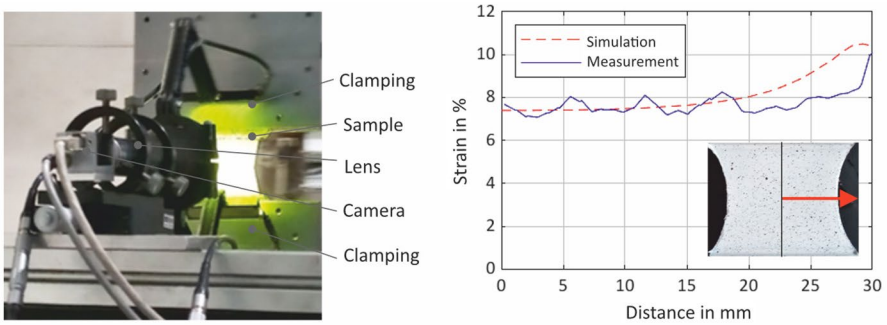

Fig. 11 Optical strain measurement setup (left) and comparison with FE-Model on the designed specimen (right)

The GOM Correlate software [45] was used to analyse the images. In Fig. 11 on the right shows the comparison between optical measurement and simulation. A uniaxial tensile load of Fy = 2970 N is applied and the logarithmic strain is compared in the plot. Due to symmetry, the comparison is shown along the path marked on the specimen geometry, unilaterally from the centre to the edge.

As shown in Fig. 11 right, the measured data agrees well with the simulation in the range of 0—20 mm distance from the centre. The strain in the measurement and in the simulation are at the same level of approximately 7.5%. This is an important finding as it ensures that the applied tensile prestress results in the desired strain rate in the test area of the composite. A slight deviation or shift can be seen in the range of 20—30 mm. This may be due to a slight offset in the measurement, but also due to the fact that a detailed measurement to the very outer edge is not possible.

Another possible deviation can be explained by the measurement compared to the simplified two-dimensional planar stress FE-Model. In this way, the simulation was verified using optical strain measurements, and more information on the methodology used can be found in [45, 46].

The simplified planar modelling of the specimen was deliberately chosen, as this is a basic study of the geometry optimisation. Parameters such as layer spacing and stress in the thickness direction were neglected for simplicity. In the future, more detailed modelling techniques will also be used to evaluate parameters relevant to damage assessment. Many different techniques can be applied, but these can lead to different results [47] and therefore an appropriate approach should be selected.

6 Experimental

6.1 Mechanical Specimen Testing

The first biaxial tests were carried out on a hexapod test rig. This type of test stand can reproduce multi-axial loading. Two of the six available axes of freedom are used to test the specimen. The available displacement and force measurement equipment on the test stand was used. Figure 12 (left) shows the test setup on the hexapod test stand. The exact test procedure and requirements are explained in more detail in the following section.

In the specimen, the stress on the fibres should be the same as in the air spring bellow to achieve comparable loading conditions and to ensure transferable results. Figure 12 (right) shows the test procedure on the developed flat specimen, which provides similar loading conditions. The first step is to apply a tensile load, which is equivalent to the internal pressure in the air spring bellows. It should be noted that the fibre angle in the air spring bellow

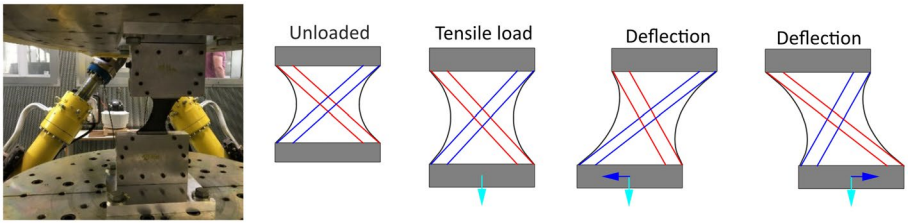

Fig. 12 Specimen testing on the hexapod test stand (left), test procedure on the flat specimen (right)

increases as the diameter increases. In the specimen, the same fibre stress is applied, but the fibre angle is reduced. This change in fibre angle can be evaluated with the FE software using a suitable composite model that allows the evaluation of the fibre angle and includes a drape simulation. The next step is to deflect the specimen in the transverse direction, equivalent to the deflection of the air spring bellows. This deflection is applied repeatedly under constant preload in order to investigate the fatigue behaviour of the cord-composite material.

As a first step pure tensile tests were carried out on the developed flat specimen. The first, simple tensile tests, consisted of a series of displacement-controlled quasi-static tensile tests and were designed to check the force transmission of the specimen clamping (force transmission from the vulcanised steel sheet to the fibres). Force and displacement were recorded in-situ during the tests. In addition, optical strain measurements on the surface were used to verify the simulation model. The test results and the surface strain measurement show, that the force transfer from the clamping plate to the composite is as designed. The clamping meets the requirements and forms the basis for further tests, for more details see [46].

Combined tensile and shear tests were then carried out for both quasi-static and cyclic experiments. The benefit of the quasi-static tests is to determine the composite Young´s modulus and further to calibrate the material model parameters. It is also possible to measure the hysteresis of the composite, the change in the fibre loading and unloading curve of the fibres. The quasi-static test also shows the static failure loads and failure modes under biaxial loading.

The benefit of the cyclic testing is to characterise the fatigue resistance of the composite to determine the tolerable load changes at different stress ratios.

6.2 Fracture Pattern Investigation

The specimen remains a prototype and its quality must be closely controlled to produce comparable and meaningful results. A method should also be used to detect delamination that allows the damage pattern to be clearly assigned. There are several possibilities for this, such as scanning electron microscopy (SEM) [48–50] or micro computed tomography (μCT) [2, 51–53]. The non-destructive method of μCT is used to avoid distortion of the damage pattern.

The density of the fibres (polyamide PA 6.6) is in the range 1.13–1.16 g/cm^3 according to the manufacturer. The density of the rubber mixture (natural rubber) is in the range of 1.25–1.35 g/cm^3 according to the manufacturer. This results in a minimum difference of 0.1 g/cm^3.

To ensure that the difference in density could be resolved, radioscopic tests were first carried out. A series of radioscopic images were then taken, followed by CT scans of selected specimens.

Due to their flexible nature, the specimens could not be placed upright on the turntable stage. Strips of balsa wood were therefore used to stabilise, the specimens, which—as they are radiolucent—had no effect on the image quality. Both the radioscopic and μCT imaging were performed on the same Phoenix v|tome|x L CT system, equipped with a 240 kV cone-beam microfocus X-ray tube operated at 120 kV and 250 μA. The experimental setup is shown in Fig. 13.

The radioscopic images were acquired with an exposure time of 500 ms and a frame averaging (image integration) of 16 images. For the CT scans, 1600 X-ray projections

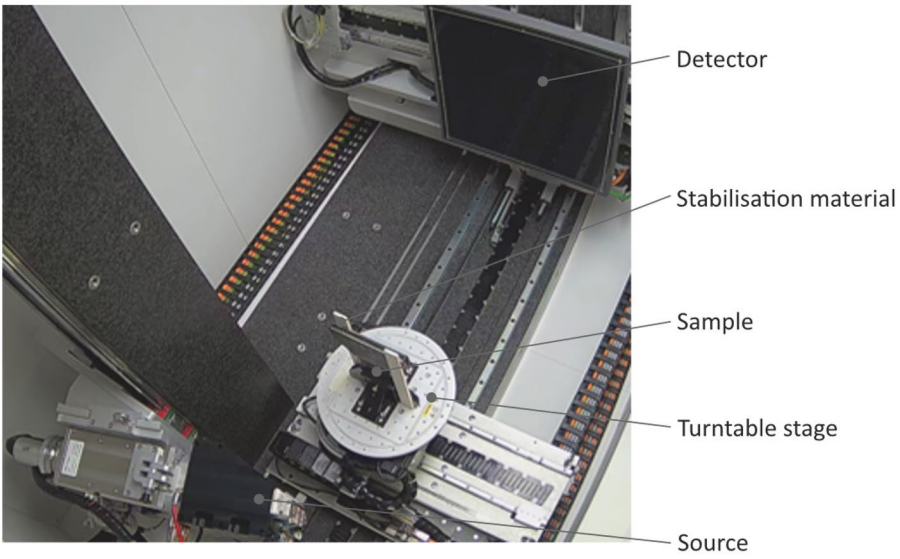

Fig. 13 Measurement setup for radioscopic and µCT imaging

were recorded in approximately 60 min using a GE dynamic 41|100 detector with 14 bit dynamic range and activated pixel binning resulting in 2000 × 2000 detector pixels.

Volume reconstruction was performed using a modified Feldkamp algorithm [54] for the filtered back projection as implemented by the system supplier. The resulting voxel size was 40 µm. The alignment and the analysis of the CT data was performed using the Volume Graphics Studio Max 3.4 software package.

The radioscopic images were cropped and digitally filtered using the FFT high-pass filter of the radiographic/radioscopic software ISee 1.11.1 [55]. The grey value look-up table was manually adjusted for optimal brightness and contrast. The FIJI distribution of ImageJ and the included directionality plugin [56] were used to analyse the specimens for fibre directions. The radioscopic images were cropped, median filtered, automatically adjusted for brightness and contrast, segmented using a local thresholding algorithm, and then analysed for fibre orientation.

7 Results and Discussion

7.1 Biaxial Cyclic Specimen Testing

As an example of the specimen testing carried out, a combined tensile and shear vibration test is described in detail in this section. The specimen to be tested, consists of two opposing layers with a fibre angle of ± 19 with respect to the vertical (see Fig. 6, left).

In the first step, the specimen is preconditioned in the tensile direction according to DIN EN ISO 2062 [57]. The specimen is unloaded and loaded twice to 1.3 times the target force and then held at the target force for 10 min. No conditioning was performed in the direction of deflection (X).

On the hexapod test stand (see 6.6.1) the tensile preload of the specimen was force-controlled, the deflection was a displacement-controlled sinusoidal signal. Test parameters: $Fy = 2970$ N, $U = 22$ mm and test frequency $f = 0.35$ Hz. The requirement was that the surface temperature should not exceed 50 °C. As the test stand was not capable of testing at a frequency higher than 0.4 Hz, no significant heating of the specimen was observed.

Figure 14 (left) shows the results of the cyclic tests on a flat specimen. The upper graph shows the extreme values of the shear forces over the load-cycles. The lower graph shows the average travel required in the direction of tension (V) to maintain the required tensile preload of $Fy = 2970$ N.

Both graphs can be divided into three areas, as is typical for the fatigue behaviour of elastomeric materials [14]. The running-in behaviour at the beginning of the test for the first 100–150 cycles, then a relatively linear range up to about 1550 cycles, followed by a slight drop, up to an abrupt rupture.

After approximately 1661 cycles, the shear force on one side drops abruptly and the tensile direction increases abruptly. This indicates that significant damage to the specimen has occurred at this point. After this test, slight bulges can be seen on the surface of the specimen, compare with the image of the specimen in Fig. 14, right. Slight damage can also be seen at the corners of the specimen, which is likely to play a minor role and is due to the unloading / compression of the material as predicted by the simulation.

The vertical force Fy is not exactly maintained at the level of 2970 N, the actual value varies between 2600 and 3250 N. The actual displacement amplitude in the transverse direction U is also somewhat larger (about 23 mm) than the specified amplitude of 22 mm ($f = 0.35$ Hz).

As can be seen from the top plot (Fig. 14, left), the shear force is not symmetrical, suggesting that the specimen has some geometric asymmetry. One possibility would be an asymmetry in fibre orientation, which will be examined in more detail in the next section.

The failure criterion is defined as a sudden drop in stiffness or a 10% drop in stiffness to determine the number of cycles to failure [22].

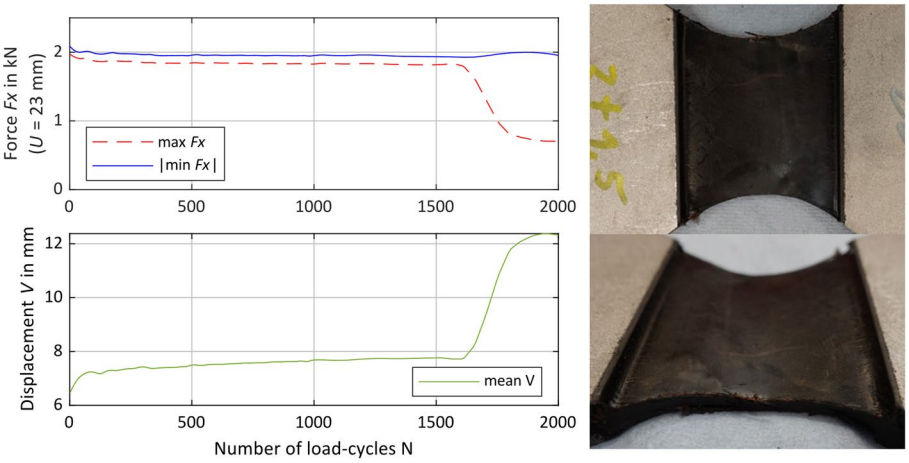

Fig. 14 Cyclic test of a flat specimen (left) and damage pattern of the tested specimen (right)

7.2 µCT Measurements

Analysis of the fracture pattern of the test specimen began with radiography as previously described.

Figure 15 shows the radiograph of the specimen examined. The image is positive, i.e. bright indicates fibres (lower density) and dark rubber (higher density). In general, deviations in fibre spacing and angle can be observed at first glance in the corner areas. In the central area examined, the fibres are evenly spaced. The requirement was a fibre angle of ± 15° in respect to the vertical direction. To verify this, an analysis of the fibre angle distribution was carried out, see also Sect. 6.6.2. This showed that the maxima of the actual fibre angle distribution were located at—19.6° and 18.6°.

Detailed analysis revealed the following: the paths marked with green lines show the areas where discontinuities in the fibres can be observed. The areas marked with circles indicate damage to the strength members, in some cases severely untwisted and damaged fibres are visible.

As a clear interpretation of the damage mechanisms is difficult with the radioscopic (2D) images alone, a 3D µCT scan of the selected specimen was also performed.

Figure 16 shows the µCT measurement on the flat specimen. In CT images bright generally means higher density and dark means lower density. Thus, in the following images, the fibres are the darker circles within the slightly lighter matrix. The slight differences in brightness between the outer and inner rubber layers show the two different

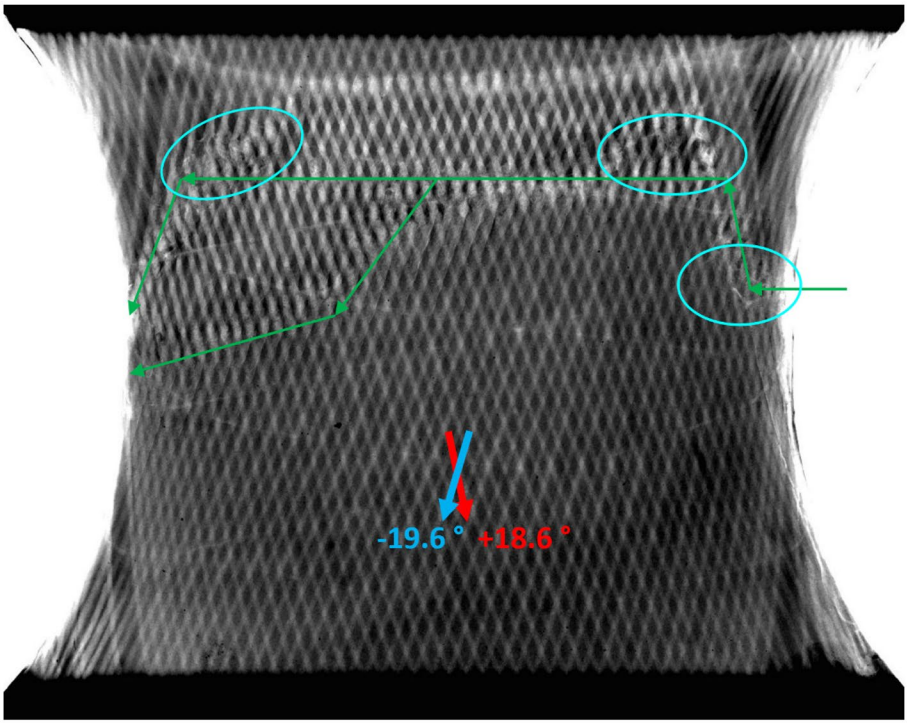

Fig. 15 Radiographic measurement (2D) with X-rays of the specimen

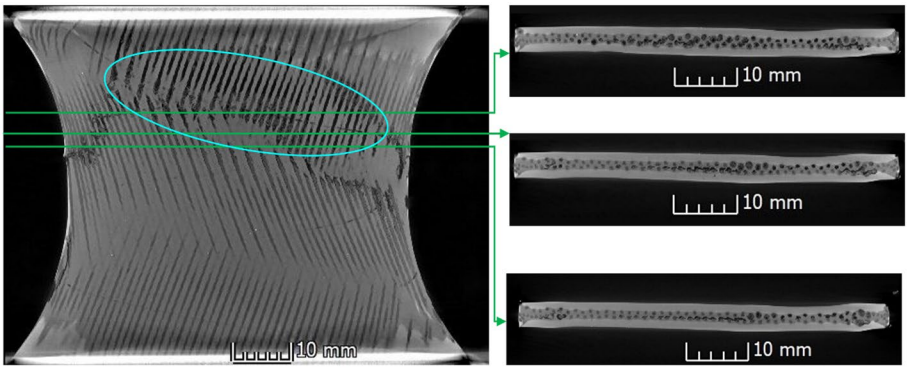

Fig. 16 µCT measurement on the flat specimen (left top view, right front views)

rubber mixtures. Very low density media (gas/air) are shown in black. The resulting voxel size of 40 µm shows both the strands and the twist of the fibres, as well as the air trapped between the strands. Two layers with two different fibre directions are visible.

In the area marked in the top view of Fig. 16 the fibres are damaged, there are dark areas indicating internal air filled volumes. The top view shows, that the outermost continuous fibres in this layer are damaged at both edges of the specimen just above the narrowest part of the specimen. in the front view, several fibres of one layer have separated from the second layer. The black lines between the fibres indicate delamination. This type of damage is clearly visible in all three front views and represents the dominant damage in this investigation. Damaged and untwisted fibres in the front view have a clearly enlarged diameter. As described above, different types of damage can be seen in the µCT measurements. These include fibre fracture and detachment of layers (delamination).

In order to better characterise the primary damage mechanism, an additional µCT measurement is shown in Fig. 17. As in Fig. 16, the damaged area has been marked in the top view. The irregular pattern in this area is indicative of damage that is better seen in the front view. The two layers of fibres are partly completely separated from each other and partly widely detached. This leads to the conclusion, that the designed

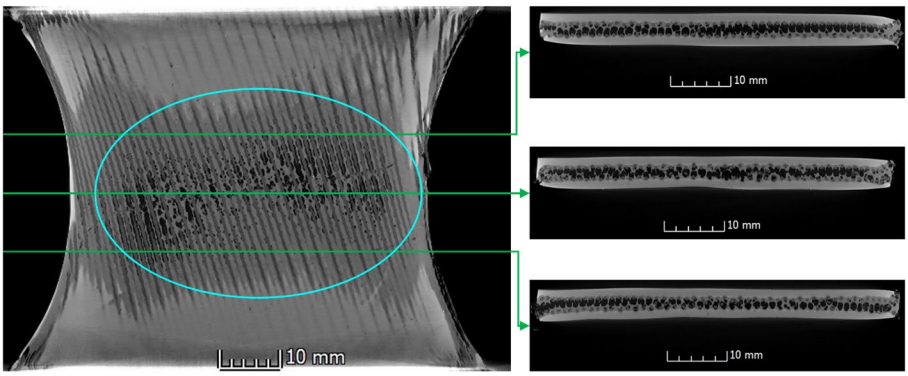

Fig. 17 µCT measurement on additional specimen tested (left top view, right front views)

specimen with the corresponding test procedure shows that the separation of the layers, delamination, is the dominant damage mechanism.

In the future, additional μCT measurements will be performed iteratively during testing to better characterise the damage progression. Several studies suggest that the damage starts at the interface (bonding agent layer) between fibre and matrix in the form of cracks [22, 58]. These are probably not visible in this dimension due to the resolution of the μCT measurement method. The abrupt jump in the measured variables in Fig. 14 indicates, that the damage occurs abruptly. It is important for this study that the delamination damage mechanism is well detectable by μCT measurement on the specimens examined.

8 Conclusions

Work on new developments and optimisations of air spring bellows for railway applications are currently performed experimentally. In general, testing of the entire air spring bellow system on a multiaxial test stand is time consuming and costly. Due to the high component and test bench costs, a representative flat test specimen has been developed to provide an efficient test methodology to facilitate an elaborated design procedure.

The most common failure mechanism occurring in the air spring bellows, the separation of the layers from each other, known as delamination, was analysed. An asymmetric tensile or compressive load on the fibre is a characteristic of this failure mechanism.

A representative specimen was designed and optimized using a two-dimensional planar stress FE-Model. A transversely isotropic material with two fibre families with an anisotropic hyperelastic material formulation is used for the fibre-reinforced rubber composite. The model has been verified by optical surface strain measurement, which shows a good correlation between simulation and measurement.

The biaxial experiments were carried out applying the developed testing methodology derived from the air spring bellow. As a final validation of the specimen geometry, a fracture pattern study was carried out, with the results showing typical signs of delamination as the dominant failure mechanism in the air-spring bellows. Radiographic analysis indicated, that it would be useful to examine the actual fibre orientation for quality control purposes.

Specimens and test methodology have been developed and validated and will be used for more extensive fatigue testing studies in the future. The transfer to the component allows a sophisticated air-spring fatigue assessment. S–N curves can be determined much more efficiently and comprehensively with this method than with whole air springs.

Funding Open access funding provided by Graz University of Technology. Partial financial support was received from Siemens Mobility Austria GmbH.

Data Availability Data will be made available on reasonable request.

Declarations

Conflict of Interests The authors have no relevant financial or non-financial interests to disclose.

References

1. Cho, J., Yoon, Y.H., Seo, C.W., et al.: Fatigue life assessment of fabric braided composite rubber hose in complicated large deformation cyclic motion. Finite Elem Anal Des **100**, 65–76 (2015)
2. Fedorko, G., Molnár, V., Živčák, J., et al.: Failure analysis of textile rubber conveyor belt damaged by dynamic wear. Eng Fail Anal **28**, 103–114 (2013)
3. Li, X., Wei, Y., Feng, Q., et al.: Mechanical behavior of nylon 66 tyre cord under monotonic and cyclic extension: Experiments and constitutive modeling. Fibers Polym. **18**(3), 542–548 (2017)
4. Naskar, A.K., Mukherjee, A.K., Mukhopadhyay, R.: Studies on tyre cords: Degradation of polyester due to fatigue. Polym Degrad Stab **83**(1), 173–180 (2004)
5. Rao, S., Daniel, I.M., Gdoutos, E.E.: Mechanical Properties and failure behavior of Cord/Rubber Composites. Appl Compos Mater **11**(6), 353–375 (2004)
6. Pelz, P., Brüger, T., Merk, J.: Numerische Festigkeitsauslegung von Luftfedern. Mater. Test. **49**(9), 447–454 (2007)
7. Pahl, H.J.: *Luftfedern in Nutzfahrzeugen*: *Auslegung, Berechnung, Praxis*. LFT Luftfedertechnik, Tönisvorst (2002)
8. Bešter, T., Fajdiga, M., Nagode, M.: Application of constant amplitude dynamic tests for Life Prediction of Air Springs at various control parameters. Strojniški vestnik – Journal of Mechanical Engineering **60**(4), 241–249 (2014)
9. Facchinetti, A., Mazzola, L., Alfi, S., et al.: Mathematical modelling of the secondary airspring suspension in railway vehicles and its effect on safety and ride comfort. Veh Syst Dyn **48**(sup1), 429–449 (2010)
10. Talasz, M.: Simulation der Bauteilsteifigkeit eines Elastomer-Faser-Verbundes, master thesis, Graz University of Technology. (2013)
11. Wode, S.: Experimentelle Untersuchungen zum Ermüdungsverhalten von Rollbalg-Luftfedern, dissertation, Leibnitz University Hannover. (1995)
12. Oman, S., Fajdiga, M., Nagode, M.: Estimation of air-spring life based on accelerated experiments. Mater. Design **31**(8), 3859–3868 (2010)
13. Förster, K.: Ein Beitrag zur Untersuchung der Lebensdauerabschätzung und des Walkverhaltens von Luftfederbälgen Mittels Statistischer Methoden. Shaker, Aachen (2012)
14. Harris, B.: Fatigue in composites. In: Science and Technology of the Fatigue Response of fibre-reinforced Plastics. CRC Press, Boca Raton (2003)
15. Oman, S., Nagode, M., Fajdiga, M.: The material characterization of the air spring bellow sealing layer. Mater. Design **30**(4), 1141–1150 (2009)
16. Shi, X., Lian, C., Shang, Y., et al.: Evolution of the dynamic fatigue failure of the adhesion between rubber and polymer cords. Polym Test **48**, 175–182 (2015)
17. Jamshidi, M., Afshar, F., Shamayeli, B.: Evaluation of cord/rubber adhesion by a new fatigue test method. J Appl Polym Sci **101**(4), 2488–2494 (2006)
18. Chandra, A.K., Mukhopadhyay, R., Bhowmick, A.K.: Studies of Dynamic Adhesion Between Steel Cord and Rubber Using a New Testing Method: PII: 0142-9418(95)00011-9. Polym. Test. **15**, 13–34 (1996)
19. Vannucchi de Camargo, F., Marcos Guilherme, C.E., Fragassa, C., et al.: Cyclic stress analysis of polyester, aramid, polyethylene and liquid crystal polymer yarns. Acta Polytech **56**(5), 402–408 (2016)
20. Averett, R.D., Realff, M.L., Michelsen, S., et al.: Mechanical behavior of nylon 66 fibers under monotonic and cyclic loading. Compos. Sci. Technol. **66**, 11–12 (2006)
21. Kenney, M.C., Mandell, J.F., McGarry, F.J.: Fatigue behaviour of synthetic fibres, yarns, and ropes. J. Mater. Sci. **20**, 2045–2059 (1985)
22. Eitzen, A., Flamm, M., Steinweger, T., et al.: On the lifetime prediction of rolling lobe air springs. Eng. Fail. Anal. **94**, 313–326 (2018)
23. Tao, Y., Windslow, R., Stevens, C.A., et al.: Development of a novel fatigue test method for cord-rubber composites. Polym Test **71**, 238–247 (2018)
24. Tian, Z., Song, H., Wan, Z., et al.: Fatigue Properties of Steel Cord-Rubber Composite. J Elastomers Plast **33**(4), 283–296 (2001)

25. Liu, Y., Wan, Z., Tian, Z., et al.: Fatigue of Unidirectional Cord- Rubber Composites. Tire Sci. Technol. **27**(1), 48–57 (1999)
26. Kottner, R., Heczko, J., Krystek, J.: Validation of identified material parameters of rubber using an Arcan shear test. Mater. Today: Proc. **12**, 404–410 (2019)
27. Hao, P., Din, I.U., Panier, S.: Development of modified Arcan fixture for biaxial loading response of fiber-reinforced composites. Polym Test **80**, 106148 (2019)
28. Almeida, J.H.S., Angrizani, C.C., Botelho, E.C., et al.: Effect of fiber orientation on the shear behavior of glass fiber/epoxy composites. Mater. Design **65**, 789–795 (2015)
29. Mandapati, R., Mallick, P.K.: A study on the biaxial fatigue of e-glass/epoxy laminates under normal and shear loadings. Int. Conf Compos. Mater. (2015)
30. Siemens Mobility Global: MoComp Bogies. (2022). https://www.mobility.siemens.com/global/en.html
31. DIN EN 13597:2008-04: Railway applications - Rubber suspension components - Rubber diaphragms for pneumatic suspension springs. (2008)
32. Karacsonyi, I.: Ermittlung der schädigungsrelevanten Beanspruchungen von Faserverbundwerkstoffen, master thesis, Graz University of Technology. (2017)
33. Polley, A.: Zur Korrelation von Simulationsrechnungen und Ausfallphänomenen bei Rollbalgluftfedern, dissertation, University of Hannover. (1999)
34. Abraham, F., Alshuth, T., Jerrams, S.: Ermüdungsbeständigkeit von Elastomeren in Abhängigkeit von der Spannungsamplitude und der Unterspannung. Kautsch. Gummi Kunstst **54** (2001)
35. DIN EN ISO 527-1-2019-12: Plastics - determination of tensile properties. (2019) https://www.beuth.de/de/norm/din-en-iso-527-1/306958894
36. Donner, H.: FEM-basierte Modellierung stark anisotroper Hybridcord-Elastomer-Verbunde, dissertation. (2017)
37. Bonet, J., Wood, R.D.: Nonlinear Continuum Mechanics for Finite Element Analysis. Cambridge Univ. Press, Cambridge (2009)
38. Holzapfel, G.A.: *Nonlinear Solid Mechanics*: *A Continuum Approach for Engineering*. Wiley, Chichester, Weinheim (2010)
39. Gasser, T.C., Ogden, R.W., Holzapfel, G.A.: Hyperelastic modelling of arterial layers with distributed collagen fibre orientations. J. R. Soc. Interf. **3**(6), 15–35 (2006)
40. Seth, B.R.: Generalized Strain Measure with Applications to Physical Problems. (1961)
41. Hill, R.: On constitutive inequalities for simple materials—II. J Mech Phys Solids **16**(5), 315–322 (1968)
42. Andreas, D.: FElupe – Finite Element Analysis, Zenodo (2022)
43. Andersson, J.A.E., Gillis, J., Horn, G., et al.: CasADi: A software framework for nonlinear optimization and optimal control. Math Program Comput **11**(1), 1–36 (2019)
44. Andreas, D.: matADi - Material Definition with Automatic Differentiation (AD), Zenodo. (2022)
45. GOM Correlate (Hotfix 6, Rev. 125216, Build 2020-02-27): GOM Software (2019)
46. Torggler, J.: Mechanisches Verhalten einer faserverstärkten Flachprobe mit Gummimatrix, master thesis, Graz University of Technology. (2020)
47. Oman, S., Nagode, M., Klemenc, J.: Rubber–fibre composite modelling and its influence on fatigue damage assessment. Fatigue Fract. Eng. Mater. Struct. **44**(2), 521–532 (2021)
48. Tonatto, M.L., Forte, M.M., Amico, S.C.: Compressive-tensile fatigue behavior of cords/rubber composites. Polym Test **61**, 185–190 (2017)
49. Jacob, H.-G.: Ein Beitrag zur Berechnung von Faserverbunden aus Elastomeren mit Polyamidfaserverstärkungen. University of Hannover, Habil (2005)
50. Tanrattanakul, V., Sungthong, N., Raksa, P.: Rubber toughening of nylon 6 with epoxidized natural rubber. Polym Test **27**(7), 794–800 (2008)
51. Castagnet, S., Mellier, D., Nait-Ali, A., et al.: In-situ X-ray computed tomography of decompression failure in a rubber exposed to high-pressure gas. Polym Test **70**, 255–262 (2018)
52. Federico, C.E., Rauchs, G., Kotecky, O., et al.: Cavitation in thermoplastic-reinforced rubber composites upon cyclic testing: Multiscale characterization and modelling. Polymer **211**, 123084 (2020)
53. Marco, Y., Le Saux, V., Calloch, S., et al.: X-ray computed μ-tomography: A tool for the characterization of fatigue defect population in a polychloroprene rubber. Procedia Eng. **2**(1), 2131–2140 (2010)
54. Feldkamp, L.A., Davis, L.C., Kress, J.W.: Practical cone-beam algorithm. JOSA A **1**(6), 612 (1984)
55. Zscherpel, U.: ISee! — the BAM radiographic image analysis software. Uwe Zscherpel. (2021). https://www.uzscherpel.de/BAM/ic/index.html
56. Schindelin, J., Arganda-Carreras, I., Frise, E., et al.: Fiji: An open-source platform for biological-image analysis. Nat Methods **9**(7), 676–682 (2012)

57. DIN EN ISO 2062:2010-04: Textiles - Yarns from packages - Determination of single-end breaking force and elongation at break using constant rate of extension (CRE) tester. (2010)
58. Pidaparti, R., May, A.: Micromechanical analysis of fatigue cracks in cord–rubber composites. Compos Struct **54**(4), 459–465 (2001)